J MATER SCI **41** (2006) 2723–2727

Size dependence of the contact angle of liquid clusters of Bi and Sn supported on SiO_2, Al_2O_3, graphite, diamond and AlN

J. MURAI, T. MARUKAWA, T. MIMA
Department of Quantum Engineering, Nagoya University, Nagoya, 464-8603, Japan

S. ARAI
1MV Electron Microscopy Laboratory, Nagoya University, Nagoya, 464-8603, Japan

K. SASAKI, H. SAKA
Department of Quantum Engineering, Nagoya University, Nagoya, 464-8603, Japan

Published online: 17 April 2006

Crystalline clusters of Bi and Sn with the diameters ranging from 100 to 5 nm were prepared by *in situ* evaporation on to different kinds of substrates in a transmission electron microscope. These metal clusters were then heated to the molten state and behaviour of the metal liquid clusters observed *in situ* in the transmission electron microscope. The contact angle of liquid clusters of Bi and Sn on different kinds of substrates changes as a function of the size of liquid metal clusters. It was concluded that the interfacial energy between the substrates and liquid metals depends on the size of liquid metal clusters and changes significantly at around 20 nm.

1. Introduction

It is well established that the thermodynamic properties, such as melting point, depend on the size of fine crystalline clusters when the diameter is, say, below 10 nm [1, 2]. These phenomena have been successfully explained by models where the structure of the surface is assumed to be different from that in the bulk solid [3]. By contrast, experimental information about liquid clusters is very limited. Merkulov and Lannin [4] performed Raman-scattering studies of liquid Bi clusters on a carbon support and have suggested that structural phase transition occurs in clusters of ∼4.5–7.5 nm in diameter.

During the course of *in situ* observation of melting processes of fine particles of Bi and Sn, it was found that the contact angle of the liquid cluster of Bi and Sn changes as a function of the size of the liquid metal clusters. This will be described in the present paper.

2. Experimental procedures

A specimen-heating holder developed by Mori *et al.* [5] based on the prototype heating holder developed by Kamino and Saka [6] was used in the present study. Fig. 1 is a schematic representation of this heating holder. Briefly, the heating holder has two fine tungsten filaments (25 μm in diameter). One heating element **1** (the upper heating element) was used for evaporation of metals, and the other heating element **2** (the lower heating element) was used for heating the substrates under consideration. In the present study particles of Bi or Sn (a few to a few tens μm in diameter) were mounted on heating element **1**, and different kinds of substrates, i.e. SiO_2, graphite, diamond, and AlN (a few μm in diameter) were mounted on heating element **2**.

First, heating element **2** was heated to clean the surface of the substrates by evaporating any volatile materials which may have formed on these surfaces. Then, heating element **1** was heated above the melting point of Bi or Sn. From the liquid droplets of Bi or Sn on heating element **1**, atoms of Bi or Sn were evaporated and deposited on to the substrates mounted on heating element **2** which was kept at a temperature below the melting point of Bi or Sn. Then, heating element **2** was heated to melt the deposited clusters of Bi or Sn on the substrates.

The microscope used was a Hitachi H-9000 NAR analytical transmission electron microscope operated at an

0022-2461
DOI: 10.1007/s10853-006-7875-y

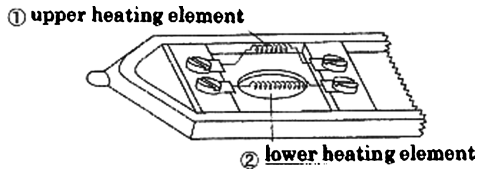

Figure 1 Schematic illustration of the specimen-heating holder used.

accelerating voltage of 300 kV. The spherical and chromatic aberraton coefficients of the objective lens are 0.69 and 1.4 mm, respectively. The point-to-point resolution of the microscope is 0.175 nm. The specimen chamber was pumped with a 340 ℓs^{-1} magnetic-bearing turbomolecular pump and kept 1×10^{-5} Pa during the *in situ* heating experiments.

3. Results

3.1. Characterization of the substrates

Figs 2a–e show typical micrographs of particles of SiO_2, diamond, graphite, AlN, and Al_2O_3 which were used as substrates, together with the respective electron diffraction patterns. The SiO_2 particles were amorphous and perfectly spherical, while diamond and AlN particles were crystalline and facetted. Graphite flake was partially graphitized.

3.2. Bi clusters on SiO_2

Figs 3a and b show low-magnification micrographs of the Bi particles supported on SiO_2 substrate before and after melting, respectively. Before melting (Fig. 3a), the Bi particles were well facetted and some of them showed diffraction contrast. After melting (Fig. 3b), the particles became perfectly spherical and showed only uniform contrast. It is noted that the positions of the Bi particles before and after melting remained unchanged and this made it very easy to compare the shapes of the individual particles before and after melting. The contact angles were measured on those particles for which the interfaces between the substrate and the particles under consideration were parallel to the incident electron beam, so that no geometrical correction was needed. Some examples are indicated by arrows.

Figs 4a and b show an example of high-resolution electron micrographs (HREM). Before melting (Fig. 4a), the cluster shows lattice fringes. At the edge of the cluster regions were observed which are referred to as "clouds" and are indicated by arrows. After melting (Fig. 4b), the cluster became perfectly spherical and the lattice fringes disappeared.

Fig. 5 shows an example of the size dependence of the contact angle of Bi liquid clusters supported on a SiO_2 substrate. It is apparent that the contact angle of smaller Bi liquid cluster B is smaller than that of larger one A. It is to be noted that Bi clusters A and B sat nearby on the same SiO_2 particle, so that their histories should have been very similar except their sizes.

3.3. Bi clusters on graphite, diamond, and AlN

Similar analyses were carried out on Bi liquid clusters supported on graphite, diamond and AlN. Figs 6a–c show HREM images of liquid Bi particles with different diameters supported on diamond substrate. It is evident that the smaller liquid particle has the smaller contact angle.

Fig. 7 summarizes the contact angle as a function of the size of liquid Bi clusters supported on SiO_2, graphite, diamond, and AlN. The contact angle of Bi liquid clusters supported on these substrates shows essentially similar behaviour, that is, the contact angle of liquid clusters of Bi remains unchanged or decreases very slowly with de-

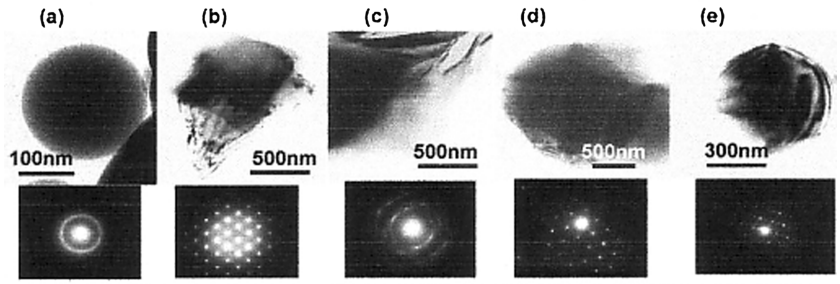

Substrate	Diameter(μ m)	Shape	Structure
(a) SiO_2	0.2~0.3	spherical	amorphous
(b) diamond	~1	facetted	single crystalline
(c) graphite	~1	facetted	polycrystalline
(d) AlN	~1	facetted	polycrystalline
(e) Al_2O_3	0.2~0.4	facetted	polycrystalline

Figure 2 Low-magnification micrographs and the diffraction patterns of the substrates used in this study (a) SiO_2, (b) diamond, (c) graphite, (d) AlN, and (e) Al_2O_3.

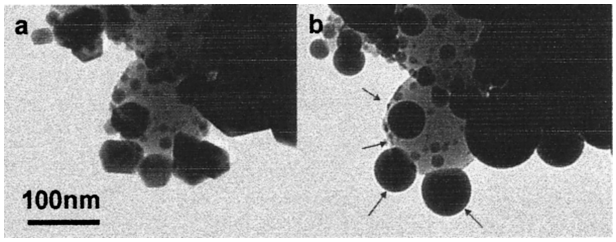

Figure 3 Low-magnification electron micrographs of Bi clusters (a) before and (b) after melting.

creasing cluster size until around 20 nm in diameter, then decreasing abruptly with further decreasing the diameter.

3.4. Sn clusters on SiO_2, diamond, and Al_2O_3

Fig. 8 summarizes the contact angle as a function of the size of liquid Sn clusters supported on SiO_2, diamond, and Al_2O_3. The liquid droplets of Sn behaved completely analogously to those of Bi, including the abrupt decrease in contact angle when the diameter decreased below 20 nm.

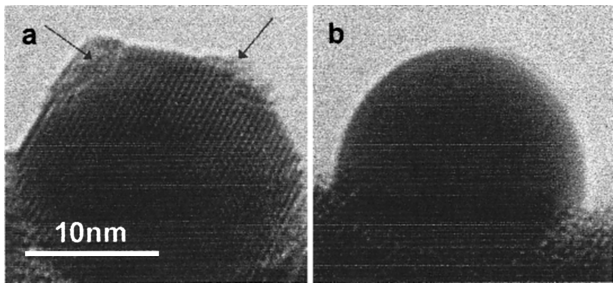

Figure 4 High-resolution electron micrographs of a Bi cluster (a) before and (b) after melting. Arrows in (a) indicate the so-called "clouds", which disappeared after melting (b).

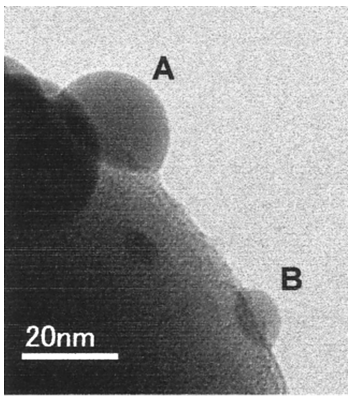

Figure 5 Example of the size dependence of the contact angle of Bi liquid cluster supported on SiO_2 substrates. The contact angle of A is larger than that of B.

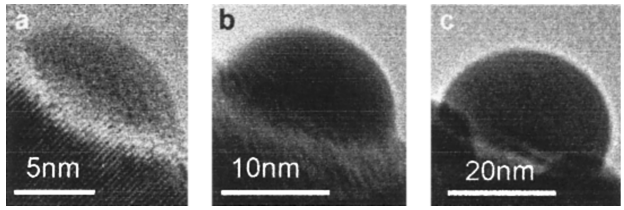

Figure 6 High-resolution electron micrographs of liquid Bi particles with different diameters supported on diamond.

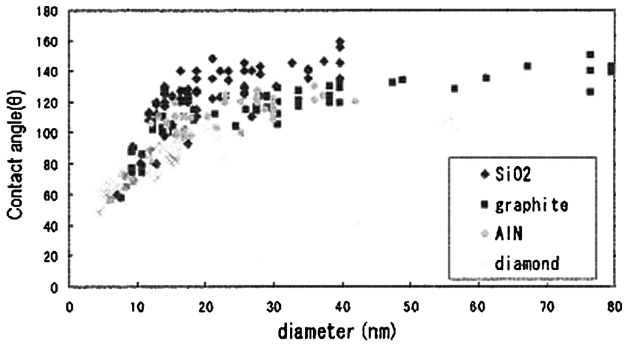

Figure 7 Size dependence of the contact angle of Bi liquid clusters supported on SiO_2, graphite, diamond, and AlN.

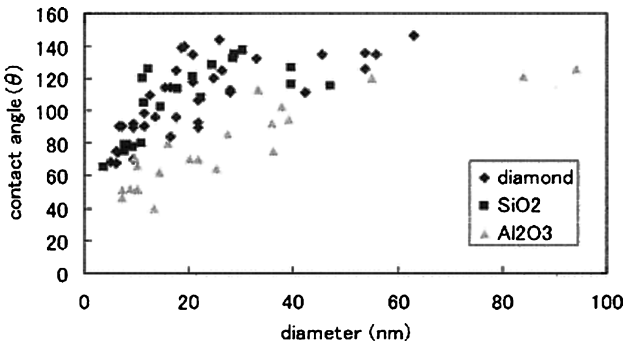

Figure 8 Size dependence of the contact angle of Sn liquid clusters supported on SiO_2, diamond, and Al_2O_3.

4. Discussion

For all the substrates studied here, the contact angle of Bi and Sn liquid clusters decreases with decreasing the size below 20 nm in diameter. However, before discussing the size dependence of the contact angle below 20 nm, it would be worth comparing the present results obtained on larger liquid clusters with those obtained on bulk liquid by the conventional methods. Table I summarizes data on contact angle of liquid Bi and Sn on different substances measured by the conventional sessile drop method. The contact angles of Bi and Sn on AlN have not been measured. The values available are in good agreement with those obtained on Bi and Sn droplets larger than 20 nm in the present study. These results suggest that the values of the contact angle obtained on droplet larger than 20 nm in the present study can be regarded as representing the contact angles of bulk liquid.

TABLE I Comparison of the values of contact angles of bulk liquids of Bi and Sn obtained by the conventional methods with those obtained on droplets with diameter larger than 20 nm in the present study (in bold)

	Substrate				
Liquid	Graphite	Diamond	SiO_2	AlN	Al_2O_3
Sn					
Previous studies	150 [7]	125 [7] 130–135 [10]	120–140 [9]	–	163 [9] 165 [8]
Present study	–	**135**	**130**	–	**130**
Bi					
Previous studies	136 [7]	106–113 [10]	–	–	–
Present study	**150**	**100**	**150**	**130**	–

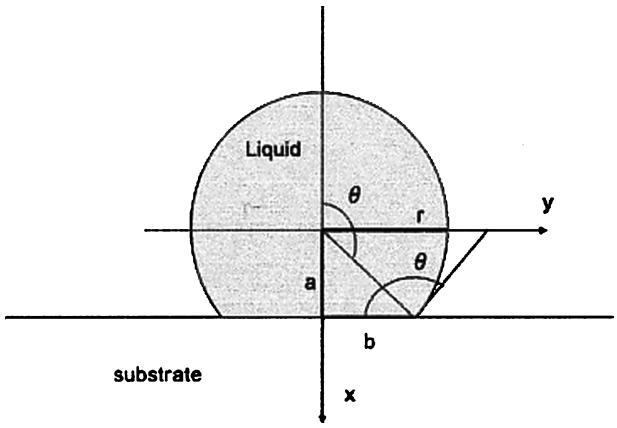

Figure 9 Geometry of a liquid cluster on a substrate.

On the other hand, the contact angles of liquid droplets of Bi and Sn smaller than 10 nm in diameter are as small as 60°. The contact angle θ is determined as a result of minimization of the total energy, F, of the system while keeping the volume of the droplet constant. Assuming the shape of the liquid-vapour interface (hereafter denoted by S_{LV}) as $y = f(x)$ (see Fig. 9)

$$F = \left[S_\infty - \pi f(0)^2\right]\gamma_{SV} + \pi f(0)^2\gamma_{SL} + 2\pi\int_a^r f\sqrt{1+f'^2}dx\gamma_{LV} + V_a g/\rho \quad (1)$$

where γ_{SV} is interfacial energy of the substrate-vapour interface (hereafter denoted by S_{SV}), γ_{SL} interfacial energy of the substrate-liquid metal interface (hereafter denoted by I_{SL}), γ_{LV} is surface energy of liquid (S_{SV}), S_∞ is the total surface area of the solid substrate before contact of the droplet and, V_a is the volume of the droplet, $\boldsymbol{g}$ is the chemical potential of the liquid phase and ρ is the density of the droplet.

Since the liquid droplet is part of a sphere, when both S_{SV} and I_{SL} are perfectly flat, Equation 1 is rewritten as

$$F = 2\pi r(r-a)\gamma_{LV} + \{S_\infty - \pi(r^2-a^2)\}\gamma_{SV} + \pi(r^2-a^2)\gamma_{SL} + V_a\mathbf{g}/\rho$$
$$= \pi A^2\gamma_{LV}(\xi^3 - 3\xi + 2)^{-2/3} \times [(2-2\xi) + \xi_\infty(\xi^2-1)] + S_\infty\gamma_{SV} + V_a\mathbf{g}/\rho \quad (1')$$

where $\xi = (a/r) = \cos\theta$ (Fig. 9), and $\xi_\infty = (\gamma_{SV} - \gamma_{SL})/\gamma_{LV}$.

Differentiation of F with respect to a leads to the following expression:

$$\frac{\partial F}{\partial a} = \left(4\pi r\frac{\partial r}{\partial a} - 2\pi a\frac{\partial r}{\partial a} - 2\pi r\right)\gamma_{LV} - 2\pi r(\gamma_{SV}-\gamma_{LV})\frac{\partial r}{\partial a} + 2\pi a(\gamma_{SV}-\gamma_{LV})$$

By setting $(\partial F/\partial a) = 0$, while keeping the volume of the droplet $V_a = \pi\{(2/3)r^3 - r^2a + a^3/3\}$ constant, the following relation, which is known as Young's relation, is obtained for the contact angle θ:

$$\cos\theta_\infty = (\gamma_{SV} - \gamma_{SL})/\gamma_{LV} \quad (2)$$

When S_{SV} and I_{SL} are not flat, Equation 2 is modified as

$$\cos\theta_r = (f_{SV}\gamma_{SV} - f_{SL}\gamma_{SL})/\gamma_{LV} \quad (3)$$

where f_{SV} and f_{SL} (>1) are factors by which the areas of S_{SV} and I_{SL} are increased.

For bulk liquid of Bi and Sn, $\theta \approx 140°$; this means that $\cos\theta < 0$ and $\gamma_{SV} - \gamma_{SL} < 0$. For liquid clusters of Bi and Sn smaller than 10 nm in diameter, θ is around 60°; i.e., $\cos\theta > 0$ and $\gamma_{SV} - \gamma_{SL} > 0$.

If $f_{SV} = f_{SL}(=f)$, that is, the roughness of S_{SV} and/or I_{SL} is same, Equation 3 becomes

$$\cos\theta_r = f(\gamma_{SV} - \gamma_{SL})/\gamma_{LV} = f\cos\theta_\infty \quad (4)$$

Since $f > 1$, roughening of S_{SV} and I_{SL} cannot explain the cross over of $\cos\theta$ from negative to positive. Com-

ing back to Equation 3, it is only when $f_{SV} \gg f_{SL}$ that cos θ_r can be close to 1. As can be seen from Figs 4–6, I_{SL} is not flat but slightly concave. This means that $f_{SV} < f_{SL}$. Thus, it is impossible to explain the change of the contact angle from the roughness of S_{SV} and/or I_{SL}.

Another possible explanation is to take the f terms to be factors by which the surface or interfacial energies themselves are modified. Among the three energies involved, i.e., γ_{SV}, γ_{SL} and $\gamma_{LV,}$ γ_{SV} is unlikely to depend on the size of a liquid droplet. Also, from Equation 2, it is clear that modification of γ_{LV} cannot lead to the cross over of cos θ from negative to positive. Therefore, the variation in the contact angle θ from 140° to 60° is to be attributed solely to a decrease in γ_{SL}. The variation in γ_{LV} may accelerate or decelerate the decrease in θ with decreasing the size of the droplets but cannot be responsible for changing the sign of cos θ.

The question remains as to why γ_{SL} decrease(s) abruptly below 10 nm. Reaction between the substrate and liquid droplets of Bi and Sn cannot explain the decrease in γ_{SL}, because HREM images of the I_{SL} show no evidence of the reaction at I_{SL}. Furthermore, there is no reason why the reaction does not take place above 10 nm, if it takes place below 10 nm.

Recently it has been shown that in the vicinity of a solid-liquid interface I_{SL} a transition layer, which is as thick as a few to several atomic or molecular layers, exists in the liquid side. Reichet *et al*. [11] observed, using the scattering of totally internally reflected X-rays, five-fold local symmetry in liquid Pb adjacent to a Si wall. Arai *et al*. [12, 13], using high-resolution electron microscopy (HREM), obtained direct evidence for existence of a transition layer in liquid of Al adjacent to a Si wall. Donnelly *et al*. [14] observed by HREM ordering in a liquid Xe confined by flat surfaces. Similarly, the structure of the liquid near the surface S_{SV} is likely to be modified. Needless to say, such modified layers in I_{SL} and S_{SV} should exist in the bulk liquid as well. However, when the size of a liquid droplet is large enough, the existence of such the modified layers in I_{SL} and S_{SV} does not affect the bulk term in thermodynamics of the wetting behaviour of a droplet, because the number of atoms (or molecules) contained in I_{SL} and S_{SV} is far smaller than the number of atoms contained in the bulk liquid. However, this would be no longer the case when the size of the liquid droplet is decreased to such an extent that the existence of the transition layers in I_{SL} and S_{SV} reduces significantly the numbers of atoms in the bulk liquid relative to the total number of atoms in the droplet. Once the size of the liquid is close to the widths of the modified layers in I_{SL} and S_{SV}, then the bulk term may virtually vanish and both of the interfacial energies, γ_{SL} and γ_{LV}, may change.

Acknowledgements

We kindly acknowledge the financial support of The Grant-in-Aids from the Ministry of Education, Culture, Science and Sports (Contract # 14205092)

References

1. G. L. ALLEN, R. A. BAYLES, W. W. GILE and W. A. JESSER, *Thin Solid Films* **144** (1986) 297.
2. M. TAKAGI, *J. Phys. Soc. Jpn.* **9** (1954) 359.
3. R. KOFMAN, P. CHEYSSAC, A. AOUJ, Y. LEREAH, G. DEUDTSCHER, T. BEN-DAVID, J. M. PENISSON and A. BOURRET, *Surf. Sci.* **303** (1994) 231.
4. V. I. MERKULOV and J. LANNIN, *Phys. Rev. B* **58** (1998) 7373.
5. H. MORI, H. YASUDA and T. KAMINO, *Phil. Mag. Lett.* **69** (1994) 279.
6. T. KAMINO and H. SAKA, *Microsc. Microanal. Microsctruct.* **4** (1993) 127.
7. JU. V. NAIDICH, *Prog. Surf. Memb. Sci.* **14** (1981) 353.
8. K. NIKOLOPOULOS, *J. Mater. Sci.* **20** (1985) 3993.
9. K. NOGI, K. OISHI and K. OGINO, *J. Jpn. Inst. Metals* **52** (1988) 72.
10. K. NOGI, Y. OKADA, K. OGINO and S. IWAMOTO, *ibid.* **57** (1993) 63.
11. H. REICHERT, O. KLEIN, DOSCH, H. DENK, M. NONKIMAKI, T. LIPPMAN and G. REITER, *Nature* **408** (2000) 839.
12. S. ARAI, S. TSUKIMOTO, H. MIYAI and H. SAKA, *J. Electron. Microsc.* **48** (1999) 317.
13. S. ARAI, S. TSUKIMOTO, S. MUTO and H. SAKA, *Microsc. Microanal.* **6** (2000) 358.
14. S. E. DONNELLY, R. C. BIRTCHER, C. W. ALLEN, I. MORRISON, K. FURUYA, M. SONG, K. MITSUISHI and U. DAHMEN, *Science* **296** (2002) 507.